INT. J. NUM. METH. HEAT FLUID FLOW, VOL. 5, 399–422 (1995)

A DIRECT NUMERICAL SIMULATION OF TRANSITION IN MIXED CONVECTION FLOWS BETWEEN TWO HEATED PARALLEL PLATES

C. C. HAO AND J. N. CHUNG

Department of Mechanical and Materials Engineering, Washington State University, Pullman, WA 99164-2920, U.S.A.

ABSTRACT

This paper seeks to increase our understanding on the fluid mechanics and heat transfer in a transitional mixed convection flow between two vertical plates. Direct numerical simulation by the spectral method, with a weak formulation, is used to solve the transient 3-D Navier-Stokes equations and energy equation. Initial disturbances consist of the finite-amplitude 2-D Tollmien-Schlichting wave and two 3-D oblique waves. The transition phenomena in a mixed-convection flow can be significantly different from the isothermal flow. Disturbance competitions among different modes are also found to be different from those known for an isothermal flow. In a mixed-convection flow, there exist thresholds for the low-mode Fourier waves. The intensified vortices are concentrated left of the central surface between the two plates. Hairpin vortices are formed with high *Ri*. Based on the flow visualization, the λ vortices are found to be staggered on the surfaces parallel to the plates. The *Ri* number seems to be the main parameter governing the transition mechanism. The *Nu* number is found to increase during transition.

KEY WORDS Heat transfer Spectral method Weak formulation Navier-Stokes Tollmien-Schlichting wave λ vortices

INTRODUCTION

The instabilities responsible for the early stages of transition to turbulence in wall-bounded shear flows are now, quantitatively, well understood. The first step, a linear stage with small disturbances, is dominated by slowly growing Tollmien-Schlichting waves propagating in the streamwise direction, and the development of these waves is described quite accurately by the classical linear stability theory. The landmark experiment of Schubauer and Skramstad[1] provided the confirmation of Tollmien-Schlichting waves in the Blasius boundary layer. Similar demonstrations for heated boundary layer have been furnished by Strazisar, Reshotko and Prahl[2].

The second stage is characterized by the instability of finite amplitude, streamwise Tollmien-Schlichting waves in response to infinitesimal, oblique disturbances (Krist and Zang[3]). It is also called the secondary instability. This type of instability induces strong vortical flow patterns in the boundary layer, the basic element of which is the λ vortex. These vortices possess regular patterns which are caused by the fundamental and subharmonic instabilities. The fundamental instability is called the K-type transition after Klebanoff, Tidstrom and Sargent[4]. Craik[5] and Herbert[6] have identified two classes of subharmonic instability, known as the C-type and H-type, respectively. The K-type transition is characterized by the growing of the ($k_x=1$, $k_z=1$) wave. k_x and k_z label the Fourier wave numbers in the numerical representations with respect to the fundamental wave-numbers in the streamwise and spanwise directions, respectively. Spalart[7] used random white noises as the initial disturbances and indicated that either the fundamental

0961–5539/95/050399–24$2.00

Received February 1993
Revised April 1994

or the subharmonic types of breakdown can appear depending on the amplitude of noises. Only the K-type transition is considered in this study because the effects of buoyancy on transition of flows are the major concerns and the effects of disturbance amplitude have been studied by Spalart *et al.*[7,8]. Therefore the initial disturbances selected in this analysis correspond to those which were known to induce K-type transition in isothermal flows.

Mucoglu and Chen[9] studied the linear stability of mixed-convection flows adjacent to a vertical isothermal surface. A forced flow was assumed to be perturbed by buoyancy effects. Later, Chen and Mucoglu[10] analyzed the linear wave instability of mixed flows over horizontal surfaces. The mixed convection studies in the past are limited to linear analyses for either forced convection perturbed slightly by buoyancy effects or buoyancy driven flow perturbed by the forced convection. There is no single study which addresses the two effects that are of the same order of magnitude. All the studies of mixed convection stability in the past were conducted by either the linear stability theory or the weakly nonlinear stability theory. Analyses on higher nonlinear stages in the transition process of a mixed-convection flow, have not been reported in the literature. Gebhart *et al.*[11] gave a most recent comprehensive review of the literature on buoyancy-driven and mixed-convection flows.

In the last decade, direct numerical simulations based on spectral methods, have been used to study the detailed structures of flows in the nonlinear stage of transition. The typical examples are given by Spalart and Yang[8] and Zang and Hussaini[12] for Blasius flows; and Orszag and Kells[13] and Krist and Zang[3] for flat channel flows. In the work of Zang and Hussaini[12], heat transfer is also included for the purpose of transition control. The rest of the transition studies were all limited to the isothermal flows. In this paper, we intend to explore the transition process in mixed-convection flows by direct numerical simulations. There are three objectives in this study:

1 Investigate the disturbance competition patterns among different Fourier modes in transition flows.
2 Study the vortices development as related to large-scale structures using particles visualization technique during the nonlinear transition stage.
3 Understand the heat transfer mechanisms during the transition stage.

COMPUTATIONAL METHODOLOGY

Problem formulation

The flow investigated is the transitional mixed-convection flow between two parallel long vertical surfaces separated by a distance $2d$. The system configuration is shown in *Figure 1*. The temperatures of the two plates are kept at T_1 and T_2 respectively. The X-coordinate is aligned with the streamwise direction, the Y-coordinate is the direction perpendicular to the walls and the Z-coordinate is the spanwise direction. The buoyancy force is aligned with the forced flow in the streamwise direction. Viscous dissipation is excluded because we are not dealing with very high Prandtl number fluids. Viscous dissipation needs to be included only when highly viscous oil is considered. The governing equations for an incompressible flow, non-dimensionalized by d (half width of the channel) and the isothermal laminar parabolic centerline velocity U_0, can be written as:

Continuity:

$$\nabla \cdot \bar{U} = 0 \tag{1}$$

Momentum:

$$\bar{U}_t + \bar{U} \cdot \nabla \bar{U} = -\nabla P + \frac{1}{Re} \nabla^2 \bar{U} + Ri \cdot \frac{T - T_r}{T_2 - T_r} \bar{i} \tag{2}$$

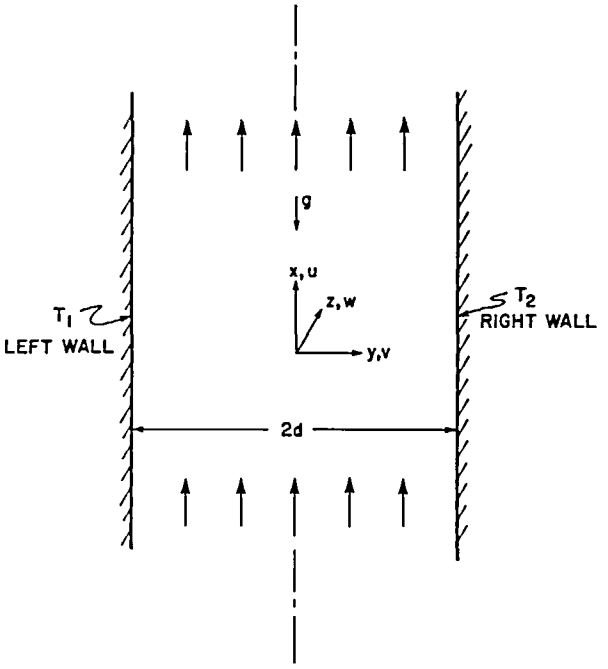

Figure 1 Schematic of the coordinate system

Energy:

$$T_t + \bar{U} \cdot \nabla T = \frac{1}{Pr \cdot Re} \nabla^2 T \tag{3}$$

where ∇P is the dimensionless pressure gradient responsible for the forced flow and $\bar{i}$ is a unit vector in the X-direction. $Re = \frac{U_0 \cdot d}{\nu}$ is the Reynolds number, where ν is the fluid kinematic viscosity. Ri is the Richardson number, defined as $Ri = \frac{dg\beta(T_2 - T_r)}{U_0^2}$ and g is the gravitational acceleration constant. $T_r = \frac{T_1 + T_2}{2}$, is the reference temperature. T is the instantaneous fluid temperature. The Boussinesq approximation is used here and β is the thermal expansion coefficient. $Pr = \frac{\nu}{\alpha_T}$ is the Prandtl number and α_T is the thermal diffusivity.

Physically the flow is driven by a combination of the pressure gradient and the buoyancy force. The pressure gradient driven flow is maintained usually by a pump and is termed the forced flow. The buoyancy driven flow is caused by the temperature gradient resulting from the unequal temperatures maintained on the two plates. The Richardson number measures the strength ratio of the buoyancy driven flow to the forced flow.

For the energy equation, it is more meaningful to rewrite (3) in terms of $\theta = T - T_m$, where T_m is the corresponding temperature profile of the steady, laminar flow which is assumed as the system condition at the beginning of the transition process. The advantage of using θ is twofold. First, it allows one to concentrate on the characteristics of temperature variations resulting from

the three-dimensional transition mechanism and to avoid obscurity caused by the laminar mean profile. Second, when heat transfer is involved, there is usually a net increase in the mean temperatures along the streamwise direction. When periodic conditions in x is applied, i.e., mean temperature is independent of x and parallel, contradiction will occur if T is used instead of θ. A similar concept was adopted by Spalart and Yang[8] for transition study of boundary layer flow, where a new velocity variable, the difference between the actual velocity and the mean velocity, was defined to account for the increase of mean velocity with the streamwise coordinate as a result of the net inflow of mass into the boundary layer. Ghaddar *et al.*[14] also defined a new temperature variable for the study of heat transfer in grooved channels. They adopted the spectral-element method and imposed periodic condition in the streamwise direction. In the current study, (3) is rewritten in terms of θ and given as follows:

$$\theta_t + \bar{U}\cdot\nabla\theta = \frac{1}{Pr\cdot Re}\nabla^2\theta - V\frac{\partial T_m}{\partial y} \tag{4}$$

where $\theta = T - T_m$ and V is the y-component velocity. T_m is the initial laminar flow temperature profile and it is derived based on steady, two-dimensional, and fully-developed assumptions. These assumptions lead T_m to become a function of y only. More details of its derivation is given later in the paper.

The boundary conditions are stated in the following:

$$\bar{U}(x,y,z,t) = \bar{U}(x+L_x,y,z,t) \tag{5}$$

$$\bar{U}(x,y,z,t) = \bar{U}(x,y,z+L_z,t) \tag{6}$$

$$\bar{U}(x,1,z,t) = 0 \tag{7}$$

$$\bar{U}(x,-1,z,t) = 0 \tag{8}$$

$$\theta(x,y,z,t) = \theta(x+L_x,y,z,t) \tag{9}$$

$$\theta(x,y,z,t) = \theta(x,y,z+L_z,t) \tag{10}$$

$$\theta(x,1,z,t) = 0 \tag{11}$$

$$\theta(x,-1,z,t) = 0 \tag{12}$$

where L_x and L_z are the domain lengths in the x and z directions. The boundary conditions at the solid walls ($y = 1, -1$) are the non-slip conditions and the prescribed wall temperature (T_2, T_1) respectively. By subtracting the T_m from T, θ will have zero boundary conditions since T_m satisfied the T_1 and T_2 boundary conditions. Periodic conditions are applied in the x and z directions. The condition of periodicity resorts to the parallel flow assumption, which is necessary because of the extreme resolution demands in the streamwise direction. Under the current computational resources, it is not yet feasible to tackle the entire spatial problem. The use of a new temperature variable, θ, certainly helps reduce the difference resulting from the parallel assumption. It has been demonstrated that numerical simulations based on the parallel flow assumption achieve good agreement with the detailed flow field structure of experimental data (Zang and Hussiaini[12]). The periodicity assumption also implies that a temporal instablity rather than a spatial instability is studied.

The initial conditions of the velocity and temperature of the laminar mean flow are $\bar{U}_m$ and T_m respectively which are derived later in details. The initial conditions of the velocity disturbances consist of a finite-amplitude 2-D Tollmien-Schlichting wave and two 3-D oblique waves as shown below:

$$\bar{U}(x,y,z,0) = \bar{U}_m(y) + \varepsilon_{2D}\bar{U}_{2D}(y)e^{ik_x x} + \frac{1}{2}\varepsilon_{3D}\bar{U}_{3D,1}(y)e^{i(k_x x + k_z z)} + \frac{1}{2}\varepsilon_{3D}\bar{U}_{3D,2}(y)e^{i(k_x x - k_z z)} \tag{13}$$

The 2-D Tollmien-Schlichting wave and two 3-D oblique waves are obtained using the ORRSOM

code developed by Lee and Reynold[15]. In the ORRSOM code, the Orr-Sommefeld equation is solved with an input of the steady state mean background flow. Here, we only investigate the momentum instability and the thermal instability is not considered. No temperature disturbance is added to the flow initially and T equals to T_m. The initial conditions are stated as:

$$\theta(x,y,z,0)=0 \tag{14}$$

In the above, k_x and k_z are the streamwise and spanwise wave numbers and are equal to one for the K-type transition. We apply the K-type transition initial disturbances and look for any deviation from the K-type transition in the mixed-convection environment. $\bar{U}_{2D}$ is the least stable two-dimensional eigenfunction. $\bar{U}_{3D,1}$ and $\bar{U}_{3D,2}$ are the three-dimensional eigenfunctions at $(k_x,k_z)=(1,1),(1,-1)$ respectively. $\bar{U}_m$ is the initial laminar steady velocity profile and the details of its derivation are showon later. ε_{2D} and ε_{3D} are chosen such that the 2-D wave amplitude is 11% and the 3-D wave amplitiude is 10% of the mean laminar velocity amplitude, respectively. The noise levels are set to be high in order to trigger the formation of nonlinear structures earlier (Krist & Zang[3]).

First the initial laminar velocity $\bar{U}_m$ and temperature T_m need to be determined. The flow can be assumed steady, two dimensional and fully developed initially. The fully developed condition implies that $\frac{\partial}{\partial x}=0$. The 2-D assumption means $\frac{\partial}{\partial z}=0$, The momentum and energy equations can then be simplified as:

$$\frac{1}{Re}\frac{\partial^2 U_m}{\partial y^2}=\frac{\partial P}{\partial x}-Ri\frac{T_m-T_r}{T_2-T_r} \tag{15}$$

$$\frac{\partial^2 T_m}{\partial y^2}=0 \tag{16}$$

Their solutions can be easily found as:

$$U_m=\frac{Re}{2}\left(-\frac{Ri}{3}\cdot y^3+\frac{\partial P}{\partial x}\cdot y^2+\frac{Ri}{3}\cdot y-\frac{\partial P}{\partial x}\right) \tag{17}$$

$$T_m=\frac{T_2-T_1}{2}\cdot y+\frac{T_1+T_2}{2} \tag{18}$$

It is noted that (17) and (18) represent the velocity and temperature profile, respectively for a laminar flow in a long channel where both flow and temperature profiles are considered to be fully developed. The Reynolds number based on the corresponding isothermal Poiseuille flow center line velocity, which is also called the nominal Reynolds number in this study, is 1500. Three Richardson numbers are studied and they are (0.005, 0.01, 0.05). The Reynolds number based on the maximum x-component velocity, will be 1875 for $Ri=0.005$, 2550 for $Ri=0.01$ and 7880 for $Ri=0.05$. All three cases are linearly unstable. The initial x-component velocities with respect to each Ri number are shown in *Figures 2–4*. The buoyancy force causes a favourable pressure gradient at the right-hand-side of the channel and induces higher velocity. This is why the local maximum Re number is increased once buoyancy effects are included. While at the left-hand-side, buoyancy force is in the negative x-direction, which tends to slow down the pressure driven forced flow or create a reverse flow if buoyancy force is larger than the pressure gradient force at high Richardson numbers. There is no reverse flow formed in *Figure 2*. In *Figure 3*, the buoyancy induces weak reverse flows. *Figure 4* shows a significant reverse flow at the left side and the buoyancy also speeds up the flow at the right-hand-side. Reversed flow may have a significant impact on the transition. That is the reason why we include cases with some reversed flows. It is noted that the flow profiles are totally different from the parabolic profile of isothermal flows.

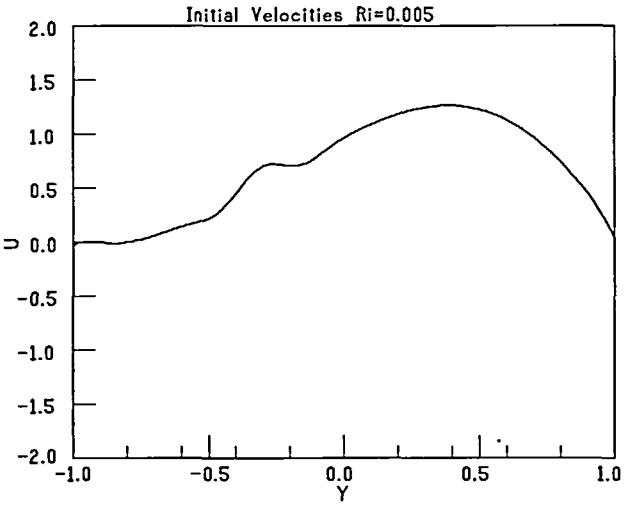

Figure 2 Initial velocity profile for $Ri=0.005$

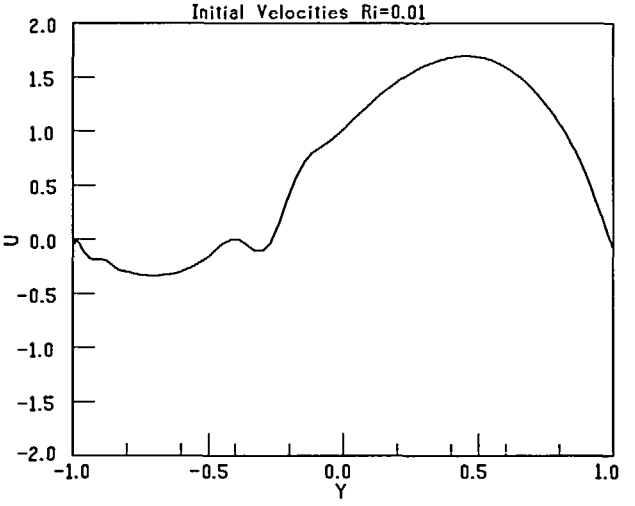

Figure 3 Initial velocity profile for $Ri=0.01$

Numerical methods

Direct numerical simulation by the spectral method with a weak formulation was employed to solve the governing equations (1), (2) and (4). The concept of spectral methods coupled with a weak formulation was first introduced by Leonard[16], later Moser *et al.*[17] applied it successfully to study the Taylor-Couette channel flow. This method offers the following advantages: increased accuracy of a spectral method; an exact implementation of the continuity and boundary conditions; simpler time-advance scheme and less storage requirement (Moser *et al.*[17]).

The weak-formulation spectral method has been proven effective by many researchers for the Navier-Stokes equation. However, we believe that this paper provides the first report on the use

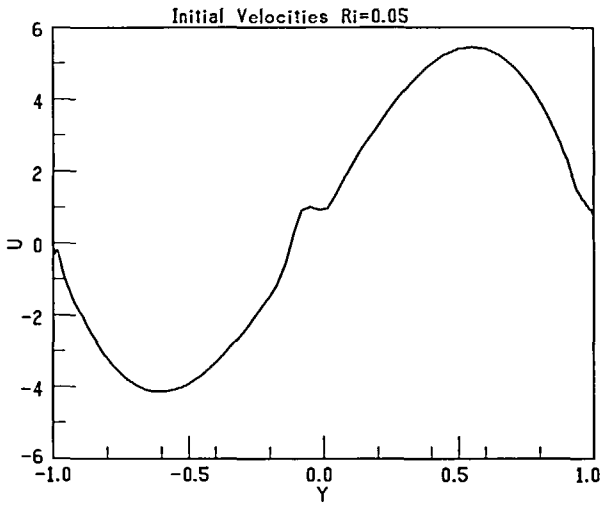

Figure 4 Initial velocity profile for $Ri=0.05$

of weak-formulation spectral method for solving coupled momentum and energy equations. Details of the weak formulation applied to coupled momentum and energy equations are given in Hao[18] and thus are not repeated here.

CODE VERIFICATION

Momentum equations

Before the Navier-Stokes equations could be solved directly by computers, the linear stability of flows has been studied using the Orr-Somerfeld equations. The Orr-Sommerfeld equation was derived by assuming that the disturbance to the flow is infinitesimal and any nonlinear term produced by the disturbance is negligible. A direct-numerical simulation code can be verified by comparing between the results of the Orr-Sommerfeld equation and those of the direct-numerical simulations under small disturbances during the linear stage.

To verify the direct simulation program we developed for the heated channel flows (HCHAN), the evolution of an oblique decaying Tollmien-Schlichting wave in a channel was computed. The computation was done for $Re=1000$, 1500, and 2000. The wave numbers are $k_x=1$ and $k_z=1$, where the Reynolds number is based on the centerline velocity and channel half width. Chebychev polynomials up to the order 32 were used. Initial conditions for the computation were obtained from an Orr-Sommerfeld eigenfunction program (Lee and Reynolds[15]). The amplitude of the disturbance was initially set to 10^{-5} so linear stability theory was applicable. The wave was allowed to evolve for 3.71 dimensionless time units. In *Figure 5*, the curves for the disturbances decaying rates were plotted. Each curve actually represents the almost overlap of four curves. These curves are the decay rates of u', v', and w' calculated by the HCHAN and the decay rate obtained from ORRSOM. The differences among them are indistinguishable in the figure. Three different Reynolds numbers were tested. As expected, the higher the Re is, the slower the disturbance decays. At the dimensionless time of 3.71, the decay rate predicted by HCHAN was within 0.025% of that obtained from the linear stability theory, and the propagation velocity was within 0.02%.

Moser *et al.*[17] did a similar test for $Re=1500$, the difference of the decay rate was within 0.2% and the propagation velocity was within 0.05% at the dimensionless time of 3.9. Comparing

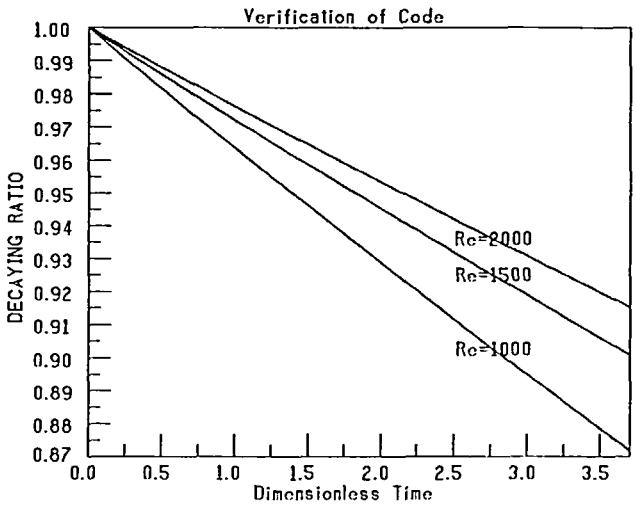

Figure 5 Verification of the computer code. That

his results to those, it is reasonable to assume that HCHAN would provide the required accuracy for the transition study..

Energy equation

The ability of HCHAN to solve the energy equation may be verified by comparing its predicted results with the analytical solution for forced laminar convection flows. For a fully-developed channel flow with viscous dissipation neglected, the temperature distribution is a linear function of the temperature on the two plates. If the initial temperature profile is modified to be different from the exact analytical solution by adding random disturbances and the product of *Pr* and *Re* falls within the range of the unconditionally stable heated flows; the code should force the temperature to approach the analytical solution after a certain time integration steps.

The initial temperature disturbances is randomly chosen. The maxium deviation of the initial temperature from the exact solution does not exceed 5%. The temperature profile calculated by the HCHAN matches the analytical solution within 0.01% after 150 time steps. The conservation of total energy of the computation box is also checked which represents that no artificial energy increase or decrease. The Nusselt number predicted by the code for constant heat flux walls agrees reasonably well with the published experimental results for a vertical annulus as shown in Hao and Chung[19]. With these, we thought that the energy equation portion is verified.

RESOLUTION REQUIREMENT

In the current study, a three-dimensional direct numerical simulation needs approximately 1–9 s.u. (service unit) on a supercomputer for the transition study. The actual time depends on the flow condition. The resolution is very stringent in transition simulation. Poor resolution will lead to an artificially chaotic state. In this study, $32 \times 52 \times 64$ is the resolution we used to allow the highest spectrum to carry energy less than 10^{-8}. The resolution in the y direction becomes more crucial in a mixed-convection flow. It is due to the highly distorted mean velocity profile along the y direction as shown in *Figure 2–4*. With a parabolic profile in the forced-convection or isothermal flow, the mean velocity is relatively smooth and less resolution in the y direction is allowed. The resolution in the spanwise direction should also be high enough to allow spanwise

structure to be simulated correctly. To reach the strongly spanwise structure stage, resolution above $64 \times 128 \times 64$ is recommended. This set of value is obtained from our experience of simulating flow at the highly nonlinear stage. We monitor the energy of the highest mode in each direction and decide to increase the resolution once the energy is larger than 10^{-8}. In order to truthfully simulate the physical mechanism, this type of monitoring must be carried out. In this paper, several different sets of physical parameters need to be studied, $32 \times 52 \times 64$ is decided to be adopted for each case in order to have conclusion and truthfully follow the physical mechanism within the allocated computing time. Higher *Ri* number will increase the requirement of resolution.

RESULTS AND DISCUSSION

Disturbance modes competition

In the study of transition, we are usually concerned with the modes competition of disturbances. An easy way to study this, is to measure the energy of each mode. Krist and Zang[3] defined the energy carried by mode (k_x,k_z) as:

$$E_{k_x,k_z}(t)=\frac{15}{16}d_{k_x}d_{k_z}\int_{-1}^{1}|\hat{u}_{k_x,k_z}(y,t)|^2dy \tag{19}$$

where:

$$d_k=2-\delta_{k,0}$$

With the initial disturbance type specified in (13), the K-type transiton is expected to appear in an isothermal flow.The K-type transition or the fundamental type of breakdown is characterized by the energy gaining mainly of the 3-D $(k_x=1,k_z=1)$ wave. The activity in the z-direction $(k_z=1)$ indicates the three-dimensional breakdown structure. In an isothermal flow, the K-type breakdown is characterized by the phenomena that the $(k_x=1,k_z=1)$ wave will finally possess more energy than the $(k_x=1,k_z=0)$ wave. The rest of the triggered waves except the $(k_x=0,k_z=2)$ one, grow initially from zero but either decay or grow at a very slow rate. The $(k_x=0,k_z=2)$ wave was found to be the fastest growing wave. In this paper, we are mainly interested in knowing how the heat transfer and buoyancy affect the K-type transition. In *Figures 6–8*, disturbance modes competition patterns are plotted for $Pr=0.7$ and various *Ri* of 0.005, 0.01, and 0.05. A Prandtl number of 0.7 corresponds to most gaseous fluids while the Richardson number represents the strength ratio of buoyancy-driven flow to that of pressure driven. The higher the Richardson number the more contribution is due to the buoyancy-driven flows. The $(k_x=1,k_z=0)$ wave grows in all the three cases. Noting that the time scale is different in these figures, it indicates that the wave gains energy much faster for higher *Ri* number. The $(k_x=1,k_z=1)$ wave is decaying in *Figures 6–7*. In *Figure 8*, it decays first and grows again after the dimensionless time passes 0.23. It is expected that the $(k_x=1,k_z=1)$ wave will not gain more energy than the $(k_x=1,k_z=0)$ wave since the latter is continuously growing in all cases. For K-type transition in an isothermal flow, the $(k_x=1,k_z=0)$ wave decays slowly to allow the $(k_x=1,k_z=1)$ wave to gain more energy after a certain time. This is the first important effect due to buoyancy which seems to suppress the three-dimensional flow development.

The $(k_x=2,k_z=1)$ and $(k_x=0,k_z=1)$ waves decay at $Ri=0.005$ and $Ri=0.01$ but grow slowly at $Ri=0.05$ after an initially decaying period. It seems that the flow could be destabilized with increasing buoyancy force. The $(k_x=0,k_z=2)$ wave is continuously growing at all cases. However, it is not the fastest growing wave as in the isothermal flow. The interesting thing is that the $(k_x=2,k_z=0)$ and $(k_x=2,k_z=2)$ waves show the existence of a threshold for their energy growth if the $(k_x=1,k_z=0)$ mode stays at relatively the same energy level. The continuously growing 2-D $(k_x=1,k_z=0)$ TS wave triggers the growing of different modes disturbances. As the 2-D TS wave attains a certain level of energy, the $(k_x=2,k_z=0)$ and $(k_x=2,k_z=2)$ modes are triggered

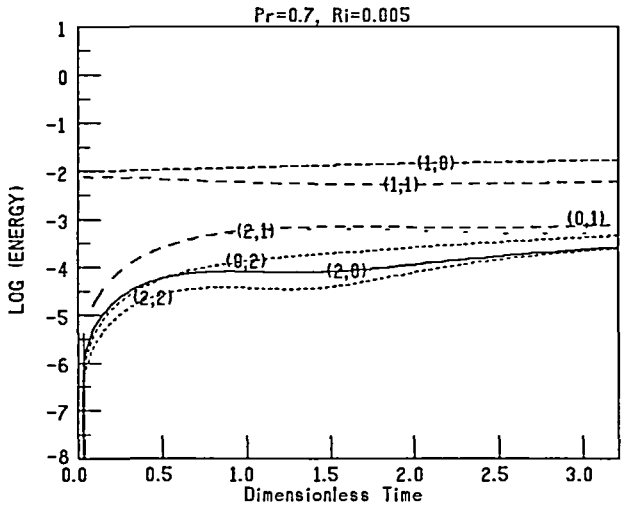

Figure 6 Modes competion curves for $Ri=0.005$ and $Pr=0.7$

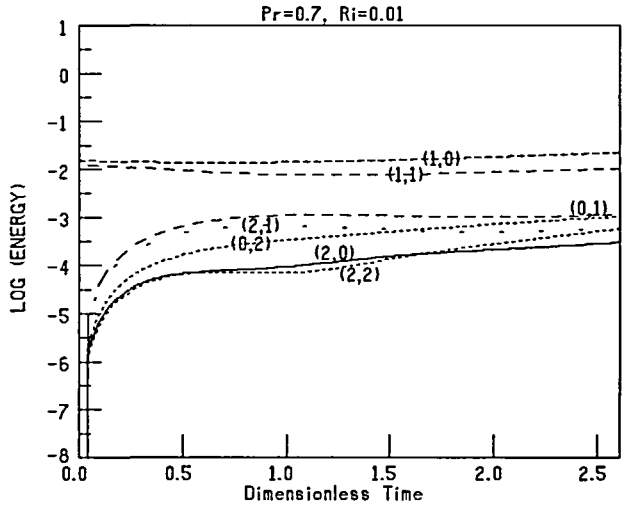

Figure 7 Modes competion curves for $Ri=0.01$ and $Pr=0.7$

and the thresholds are passed. It is seen that the ($k_x=2,k_z=1$) and ($k_x=0,k_z=1$) modes show a similar threshold phenomena, their further growth depends on whether the 2-D TS wave reaches a certain higher level as evidenced in *Figure 8*. The fastest growing waves seem to be the ($k_x=2,k_z=0$) or the ($k_x=2,k_z=2$) wave. The magnitude of the Ri number is indeed an important factor in the transition process. High buoyancy force destabilizes the flow and the continuously growing 2-D TS wave triggers different mode disturbances to break through their thresholds. All the disturbances are growing at $Ri=0.05$ which is the highest buoyancy level in the current analysis. It indicates that the flow is strongly unstable at $Ri=0.05$. With a strong buoyancy, the flow is unstable to all the disturbance waves. The unstable flow will induce fast growing disturbances and the disturbance themselves will change the flow pattern. Based on the calculated

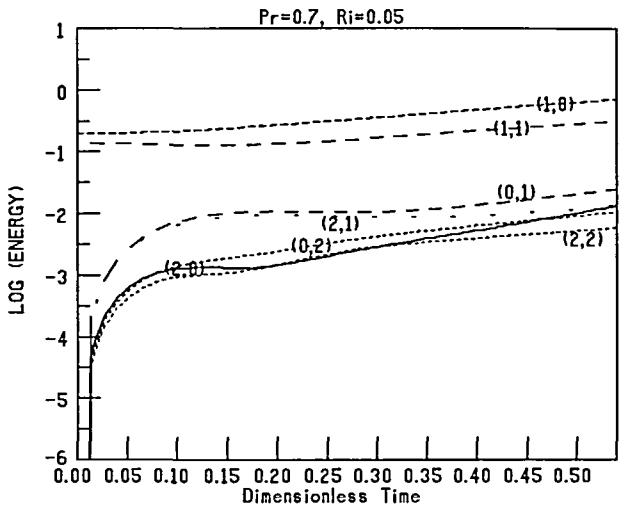

Figure 8 Modes competion curves for $Ri=0.05$ and $Pr=0.7$

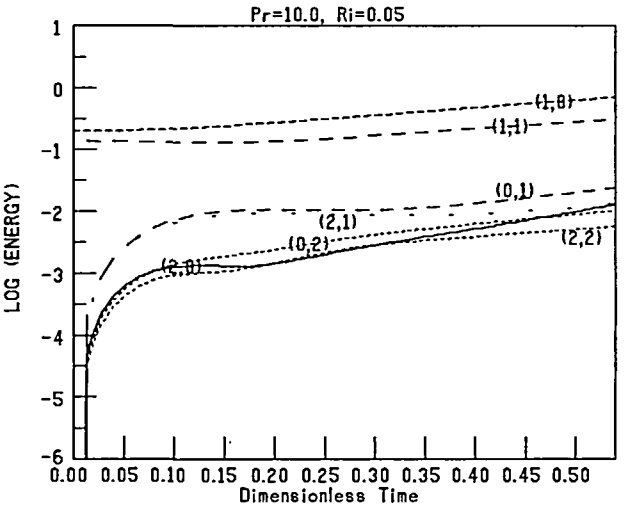

Figure 9 Modes competion curves for $Ri=0.05$ and $Pr=10$

information, one may expect that a full-developed mixed-convection flow hardly exists. This is a new result to us since there is no such equivalence in isothermal flows. Yao[20] found that the mixed-convection flow in a vertical pipe is unstable to disturbance with relatively low magnitudes by the linear stability theory. He predicted that the flow will never become full-developed. The flows he studied are at very low *Re* numbers. The direct numerical simulation study here also confirms his views in the nonlinear transition region with much higher *Re* numbers and different *Ri* numbers.

We were wondering whether the patterns of modes competition would be different for other *Pr* numbers. We next study the cases of ordinary water ($Pr=10.0$) and liquid metal ($Pr=0.001$) The *Ri* number is kept at 0.05. Comparing *Figures 9, 10* with *Figure 8*, it may be concluded that

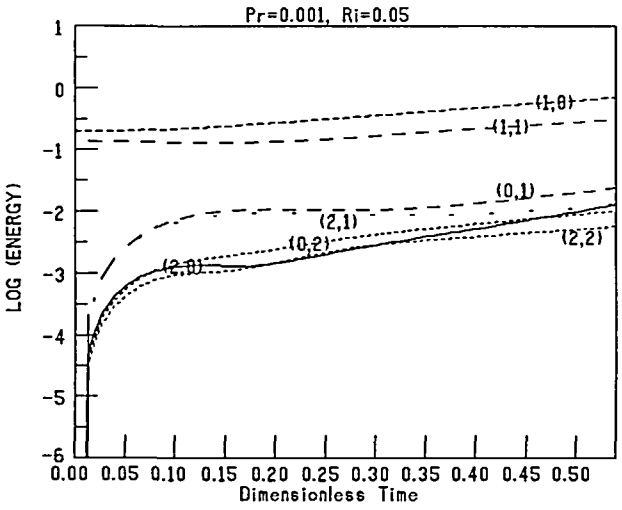

Figure 10 Modes competion curves for $Ri=0.05$ and $Pr=0.001$

there is no significant difference for various Pr numbers. The actual numerical values for the energy were further compared and the differences are on the order of 10^{-4} and the corresponding velocity differences are on the order of 10^{-2}. Based on the numerical results, we may summarize as follows:

1 The $(k_x=1,k_z=0)$ Tollmien-Schlchting wave is an unstable disturbance mode in a mixed-convection flow even without any 3-D disturbances imposed.
2 Thresholds exist for certain disturbances to grow further.
3 The transition mechanism mainly depends on the Ri number and weakly depends on the Pr number.

The first statement implies that the 2-D TS wave itself is unstable. In any isothermal flat channel flow, the 2-D TS wave will decay if 3-D disturbances are not imposed into the flow. Here the 2-D TS wave is unstable and gains more energy from the mean flow as the flow develops. It will induce large-scale 2-D periodic motions without 3-D disturbances. The second statement says that the growing 2-D TS wave will trigger different disturbances mode to grow also through nonlinear interactions. Each mode has its own threshold. The third statement indicates that the transition process mainly depends on the order of magnitude of the buoyancy force and the Pr number is only a minor factor. It can also be explained through the fact that transition is rather sensitive to the mean flow profile. Higher Ri number flow possesses a stronger inflection point in the mean flow profile and makes the flow more unstable. The initial mean flow profile in this study depends on the Ri number rather than the Pr number since constant wall temperature boundary conditions was assumed. The Pr number affects the temperature variations of the flow in a slow diffusion way. The transition process is basically a momentum exchange flow phenomena, in which the imposition of external forces in the momentum equation will result in direct effects. The Prandtl number measures the ratio of momentum diffusion effectiveness to that of the heat diffusion. The heat diffusion is generally a slower process and its effects on the flow is indirectly through the energy equation. This may explain why the Pr number turns out to be a less important parameter in the heated transition process.

Gebhart *et al.*[11] claimed that the abundant experimental data for flows subject to both natural and controlled disturbances indicate that a simple sinusoidal form of the most highly amplified disturbances is retained during transition. The flow geometry they adopted is a single vertical

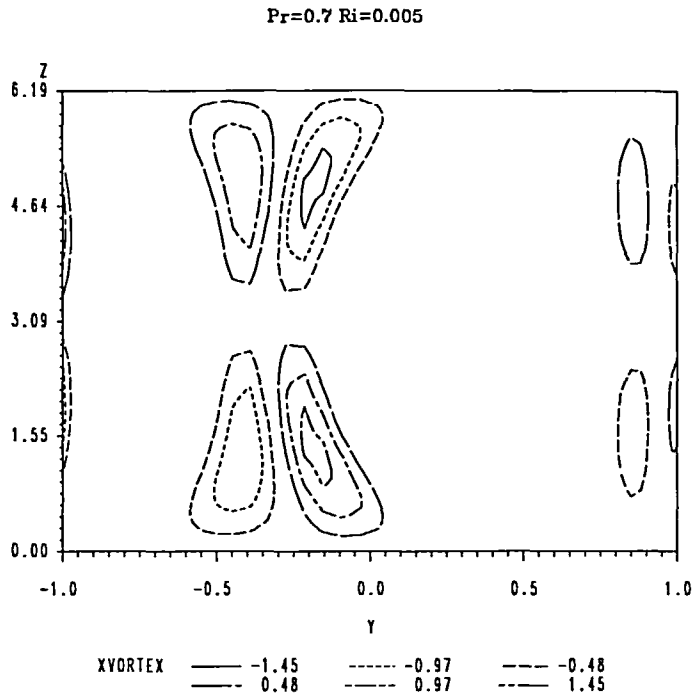

Figure 11 Streamwise vorticity contours for $Ri=0.005$ and $Pr=0.7$

plate. The mixed convection vertical transition flow between two plates we study here, also shows this same character. In our 3-D direct numerical simulation, the 2-D ($k_x=1,k_z=0$) is amplified when the flow is evolving and retained all the way through nonlinear transition stage. With the K-type initial condition, no K-type isothermal transition pattern was observed.

Streamwise vortex contour

The streamwise vortex development is an important mechanism in transition. The streamwise vortex redistributes tangential momentum across the flow. The function of an experimentally observed double vortex system in a natural convection external boundary layer was explained by Gebhart *et al.*[11]. The outer vortex convects higher-velocity fluid outward and inward from the quiescent ambient. The inner vortex does just the opposite by convecting fluids from one side to the other side. However, the flow between two vertical plates has no quiescent ambient environment and the temperature boundary conditions at the two plates also cause both favourable pressure gradient and adverse pressure gradient in the flow.

For an isothermal flow, the streamwise vortex at the laminar stage, keeps a regular pattern without being lifted. At the early nonlinear stage, the streamwise vortices will be lifted but the intensity is low. At the later transition stage, the flow will be separated right on the critical layer which is induced by the strong enhancement of the streamwise vortex with high intensity. We are interested in observing how the streamwise vortices develop in a mixed-convection flow.

In *Figures 11–13*, the streamwise vortex contours are plotted for ($Pr=0.7,Ri=0.005$), ($Pr=0.7,Ri=0.01$) and ($Pr=0.7,Ri=0.05$) cases. The streamwise vortex contour plots for the three cases are not at the same time. It is because we terminate each simulation when the resolution ($32\times52\times64$) is not sufficient to truthfully follow the real physical mechanism. The

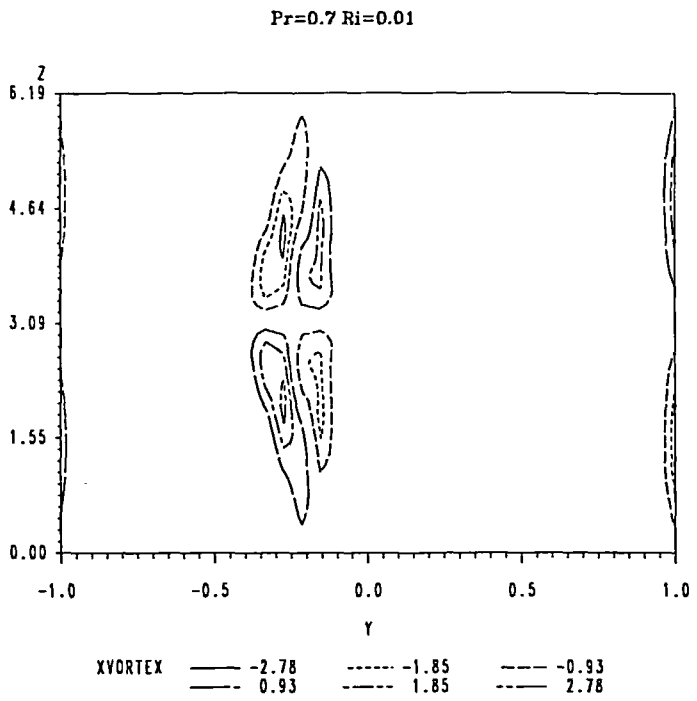

Figure 12 Streamwise vorticity contours for $Ri=0.01$ and $Pr=0.7$

time period of the higher Ri number case will be shorter. The streamwise locations of those plates were chosen such that the vortex interactions were most active. From *Figure 11*, we find that the double vortex system formed near the left of the central surface. The tangential momentum across the walls is redistributed in the double vortex system. We note that the double vortex system can be formed in different places between the plates. The double vortex systems are located close to the centerline between the walls. The vortex system can also be formed near the walls. These vortices are usually in pairs, for each pair, their circulations are relatively identical in strength but opposite in sign. A vortex convects lower-velocity fluid outward and the higher-velocity fluid inward. There will be a corresponding one doing the opposite. A vortex also convects fluids from one side to the other side. There will be a corresponding one going the other way. This type of motion enhances the possibility of layer separation. This layer will be positioned between the inner and outer vortex. In *Figure 11*, it is located at about $y=-0.25$. This layer is usually called the critical layer. Flow will be separated on this layer first and are lifted. A hairpin vortex will be formed and finally turbulence burst appears. In *Figure 12*, the streamwise vortex contour for $Ri=0.01$ is shown. Higher buoyancy force can destabilize the flow if it causes an adverse pressure gradient. Comparing *Figure 11* with *Figure 12*, the magnitude of the vortex increases and the shape of the contour becomes narrower and less regular as Ri is increased. The streamwise vortex contour at every higher Ri number is plotted in *Figure 13*. Except the large increase in the magnitudes, the vortices are lifted and ready to form the hairpin vortice. The critical layer is very close to the point of separation. The increase of the Ri number leads to an earlier transition and possible turbulence bursting as indicated by the tendency of the paired vortices to form the hairpin vortices.

From *Figures 11–13*, it is clear that the right half of the vortex structures are depressed. This may be explained as that the buoyancy force at the right-half of the channel is in the direction

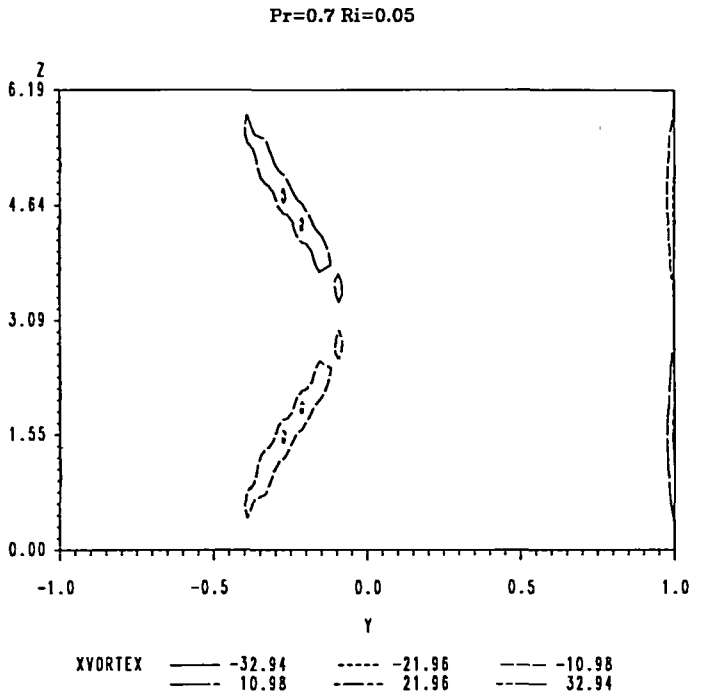

Figure 13 Streamwise vorticity contours for $Ri=0.05$ and $Pr=0.7$

of the streamwise momentum force, which induces a favourable pressure gradient. It has the effect of laminarizing the flow as the formation of streamwise vortices and the lifting tendency are suppressed. On the contrary, on the left-half of the channel, the vortices are lifted up and the vorticities are intensified because the buoyancy force gives the flow an adverse pressure gradient, destabilizing the flow. The higher the Ri number is, the stronger the pressure gradient is induced. The centerline is the interface between the favourable and adverse pressure gradient. This special setup is responsible for the vortex concentration near the centerline. The possibility of using buoyancy in transition control was shown by the linear stability theory. Here, we demonstrate that the transition can still be controlled at the early nonlinear stage by the buoyancy.

With the results from the disturbance modes competition, we conclude that the transition is mildly dependent on the Pr number and mainly on the Ri number. We also compare the vortex contours among ($Ri=0.05, Pr=10.0$), ($Ri=0.05, Pr=0.001$) and ($Ri=0.05, Pr=0.7$) cases. The results further confirmed the earlier conclusion that Ri number is the major factor in the mixed-convection transition process.

Flow visualization

Vizualizations of the flow using passive particles will be discussed next. This is similar to smoke or dye visualization in an experiment. The motion of particles is computed using linear interpolation in space and the Euler scheme in time. *Figure 14* shows the initial position of the particles. Eight spanwise lines of 64 particles each are released at regular intervals in x. The height of particle release is adjusted so that the particles are near the critical layer when breakdown occurs. This is important; by keeping the particles in phase with the flow structures one greatly enhances the correspondence between the particle-line patterns and these flow structures. The

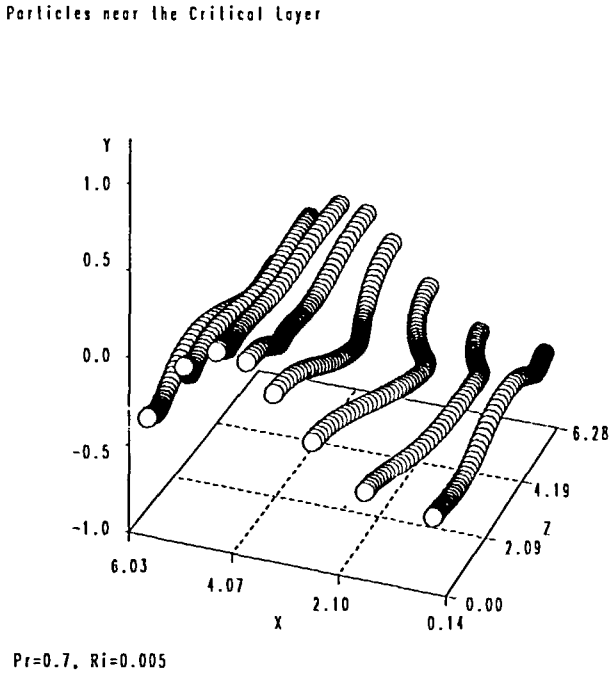

Figure 14 Flow visualization for $Ri=0.005$ and $Pr=0.7$

particles cannot be placed exactly on the critical layer, because this layer moves up and down as the flow evolves.

For each case, the distribution of particles at the end of the simulation is plotted. *Figure 14* shows the particles at ($Pr=0.7, Ri=0.005$). Looking at the picture from the point of view of the z-axis, we find that the large-scale motion is oriented in the x-direction. It is the growing 2-D TS wave that induces the regular periodic motion in the streamwise direction. This periodic motion is more substantial than the corresponding one in an isothermal flow because the 2-D TS wave there decays after a certain time. From the point of view of the x-axis, we see the particle lines are lifted up and taken down. The particles below the surface are indicated by the dark portions on the tubes. It is the vortices that stretch the particles. The projection of the particles from the y-axis is shown in *Figure 15*. The λ vortex is clearly indicated and the vortex pattern is a staggered one. This pattern is different from the pattern of the fundamental and subharmonic λ vortex pattern in an isothermal flow. The well-aligned pattern of K-type λ vortices is not observed even with the initial K-type transition input. Spalart and Yang[8] used white noise as the initial condition and they found that the actual transition breakdown pattern is more likely a mixture of the well-aligned K-type and staggered pattern. It seems that in a mixed-convection flow, the K-type breakdown pattern does not exist either. Particles are placed in the flow field initially in the form of eight spanwise lines of 64 particles each. These lines are spaced equally in the x-direction. In the y-direction, 52 layers were used and only the most interesting patterns which are usually found near the critical layers, are shown here. From *Figure 15*, we can also see the particles are moving toward the higher-vorticity region. The enhancement and distorted streamwise vortex indeed cause a regular vortex pattern on the x-z surface. The visualization of particles for the cases of ($Pr=0.7, Ri=0.01$) and ($Pr=0.7, Ri=0.05$) are given in *Figures 16–19*. In *Figures 16–17*, the 3-D visualizations all show the regular periodic

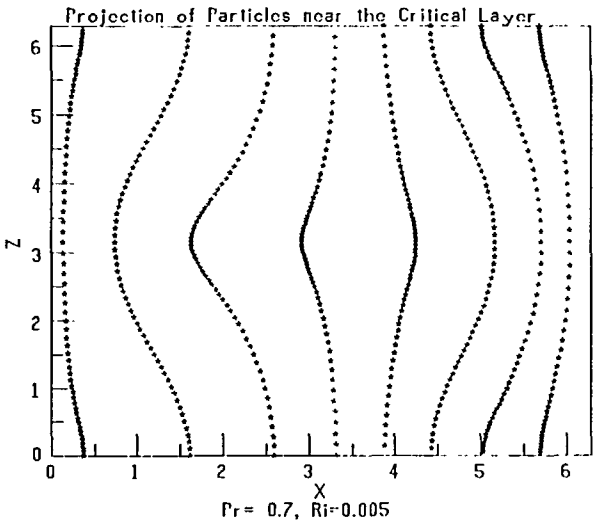

Figure 15 Projection of flow pattern near the critical layer for $Ri=0.005$ and $Pr=0.7$

motions in the x-direction. The simulations were ended at different time and the 2-D TS wave speeds are different for each case because the initial mean velocity profiles are different. These are the reasons why they are not in phase in *Figures 14,16,17*. The large-scale regular periodic motions exist in all cases. What needs to be noted is the strong variation in the y-direction shown in *Figure 17*. This is an indication of the enhancement of the vortex lift-up and distortion of the streamwise vortex. It can be expected that the hairpin vortex will be formed shortly. Due to the computing resources limitation, we are unable to conduct the simulations up to the turbulence bursting region. The projections of particles on the x-z planes corresponding to *Figures 16–17* are plotted in *Figures 18–19*. In *Figures 18–19*, the λ vortices are staggered too. This further confirms our earlier conclusion that the transition breakdown pattern is more likely a staggered one in the mixed-convection flow.

Any detailed comparison among the patterns in the three different Ri number cases will not be valid to tell the effects of the buoyancy because the critical layer is almost impossible to predict. The effects of buoyancy is best shown if the flow stuctures of the critical layer could be displayed by the particles. In our simulations, we first release the particles at 52 different positions in the y-direction. Visualizing the particle patterns on these surfaces can roughly tell where the critical layer is most likely located. The surface having the most strong vortices was then determined as the surface on which particle patterns are finally plotted. This technique of searching for the critical layer definitely requires significant amount of computing resources but it is important to visualize the particles near the critical layer.

For different Pr. numbers, we did not notice any significant variations on the particle visualization patterns. For constant wall temperature boundary conditions, the Pr number is definitely not an important parameter in the transition process.

Heat transfer coefficient

The heat transfer mechanism in a transitional flow has not been clearly understood in the past. Most of the data were collected by experiments and, in general, they are not consistent. This inconsistence is expected since transition is a complicated phenomena. The factors affecting the mechanisms include the type of disturbances, flow geometry, heating conditions, and flow

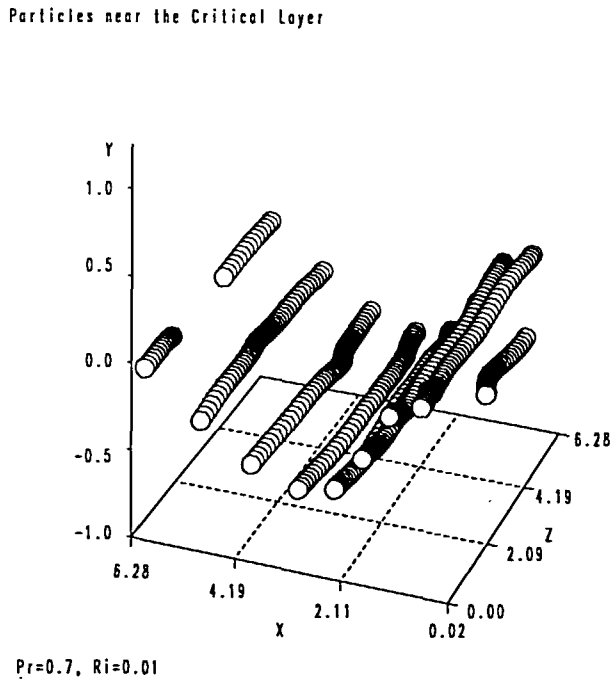

Figure 16 Flow visualization for $Ri=0.01$ and $Pr=0.7$

properties. Especially the disturbances are very difficult to control in an experimental measurement. Here we are trying to provide an accurate study based on a fixed geometry, fixed initial disturbances, and heating boundary conditions. The Nu number is defined as $Nu=\frac{hd}{k}$, where h is the heat transfer coefficient and k is the thermal conductivity. The h is evaluated as $sign(y)k\frac{\partial T}{\partial y}|y=\pm 1/(t_w-T_b)$ where T_b is the bulk temperature defined as $\frac{\int_A TUdydz}{\int_A Udydz}$. There is a local Nu number at each collocation point on the walls. In this study, the Nu number shown is an average over the x-z planes at the walls of the computation box.

First, we present the ratio of the calculated Nu number during transition to its initial value. The Nu number was written every two time steps. The initial value here means the Nu number at the second time step for each case. The period of a time step is varied from one step to another step and from one case to another case (i.e. (Pr,Ri)). This is because the period of any time step is calculated from the C_0 number. This implies that the initial Nu numbers for each case are not at the same time. We define Nu ratio to be $\frac{Nu}{Nu_{\text{initial}}}$ in order to let every curve start from 1.0. $\frac{Nu_{\text{initial}}}{Nu_{\text{m}}}$ ratios are given in *Table I*. Nu_{m} means Nu number at the laminar state. With this table, the instantaneous Nu number of a specified case can be obtained by referring to the $\frac{Nu}{Nu_{\text{initial}}}$ figure and the $\frac{Nu_{\text{initial}}}{Nu_{\text{m}}}$ table.

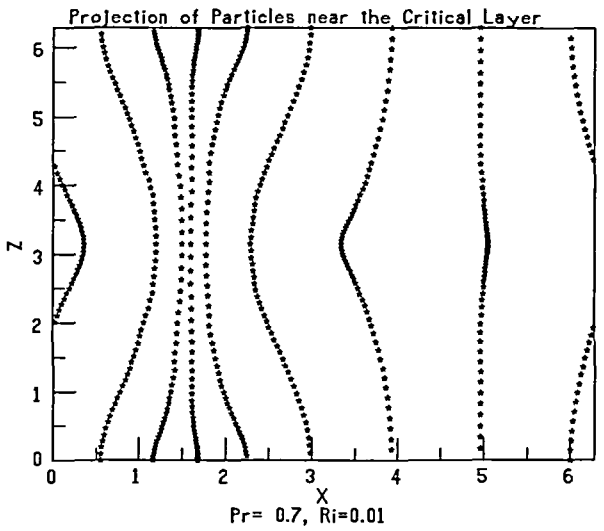

Figure 17 Projection of flow pattern near the critical layer for $Ri=0.01$ and $Pr=0.7$

Table 1 $\frac{Nu_{initial}}{Nu_m}$

Pr	$Ri \times 10^3$	Left Wall	Right Wall
0.001	50	1.000121	1.000059
0.7	50	0.999998	1.000193
10	50	0.999971	1.000092
0.7	10	0.996843	1.002787
0.7	5	0.983296	1.011356

By plotting the ratios, we are able to show explicitly the enhancement of heat transfer resulting from the unsteady transition process in a mixed-convection flow. *Figure 20* shows the *Nu* number ratio for the right wall with three *Ri* numbers of 0.005, 0.01, and 0.05; and a fixed *Pr* of 0.7. In general, the transition *Nu* number is larger than that of the initial laminar flow and the enhancement increases with the *Ri* number. The exception is that the ratio goes slightly below unity until 1.5 dimensionless time and then it starts to rise continuously for *Ri* number of 0.005. In order to explain the *Nu* number results, we need to single out the two dominant mechanisms which control the convection heat transfer process near the right wall boundary. The first is the favourable pressure gradient induced by the buoyancy which imparts a positive streamwise motion as shown in *Figure 2–4*. The second mechanism is the increased flow which enhances the heat transfer, in the meantime, also hinders the transition process or relaminarizes the transition process. These two mechanisms usually compete with each other and the relaminarization is only significant for small *Ri* number flows, for example, the *Nu* number ratio initially decreases slightly below unity for $Ri=0.005$, which is due to the effect of relaminarization. Other cases in *Figure 20* are all dominated by the increased streamwise flow which induces higher local Reynolds number and, therefore, enhances the transition process. For the average *Nu* number on the left wall boundary, the buoyancy force induces an adverse pressure gradient which weakens the forced flow and even causes a reverse flow for $Ri=0.05$ (see *Figure 4*). This adverse pressure gradient

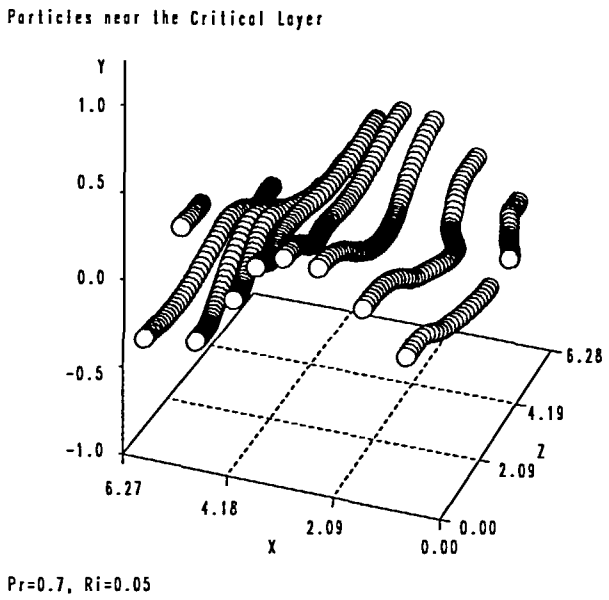

Figure 18 Flow visualization for $Ri=0.05$ and $Pr=0.7$

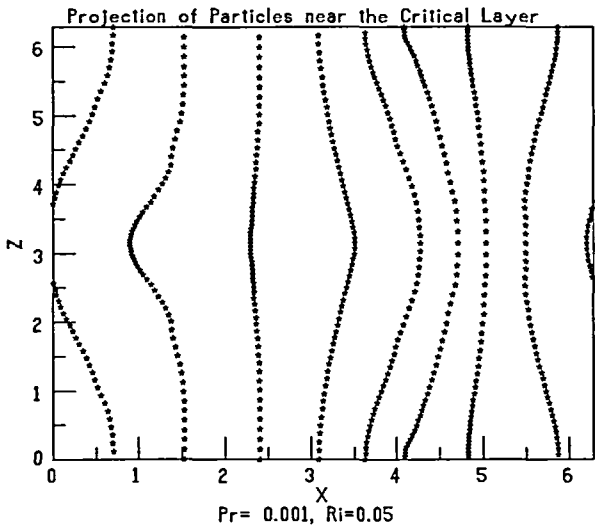

Figure 19 Projection of flow pattern near the critical layer for $Ri=0.05$ and $Pr=0.7$

helps produce a steeper velocity gradient across the channel width which promotes the transition process. The weakened streamwise flow or the reverse flow generally reduces the *Nu* number. Again the two opposing mechanisms are competing with each other and, for most parts, the mechanisms of transition prevail as far as the heat transfer is concerned. This is shown in *Figure 21* where the *Nu* number ratio is greater than unity for all three cases during the entire period of numerical simulation. Especially for $Ri=0.05$, the transition enhancement dominates

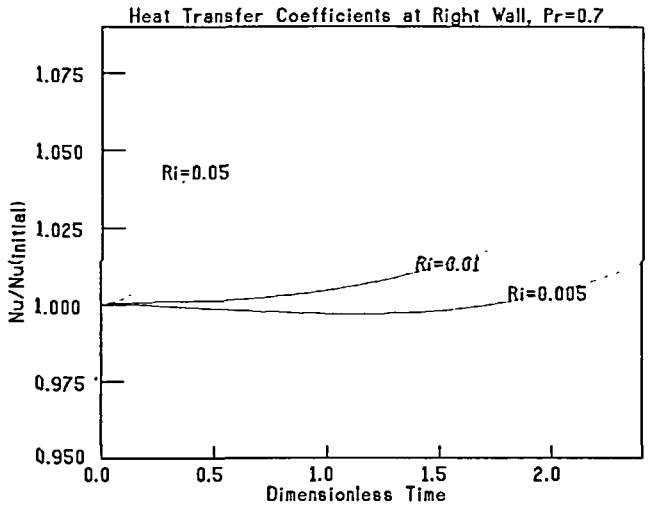

Figure 20 Nusselt Number ratio as a function of time at the right wall for $Pr=0.7$

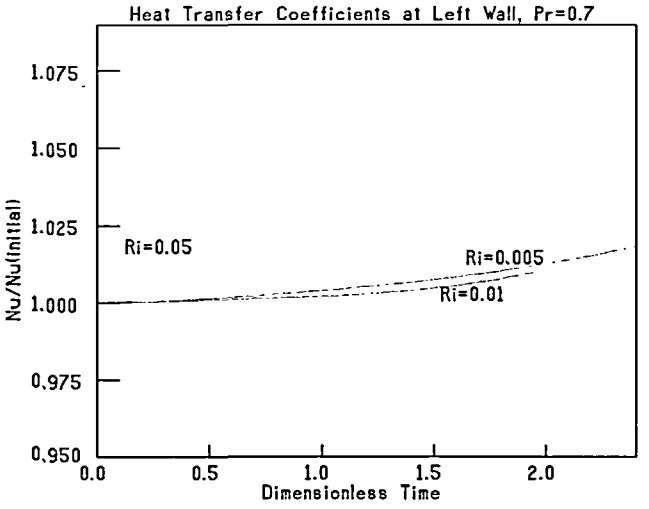

Figure 21 Nusselt Number ratio as a function of time at the left wall for $Pr=0.7$

over the reduction due to weakened streamwise flow. The ratio of the Nu number rises sharply above unity which indicates that the transition process proceeds faster and more intensively, even though the streamwise is reversed which is supposed to reduce the Nu number. For $Ri=0.005$, and 0.01, the two opposing mechanisms are of the similar order of magnitude. The ratio of the Nu number is greater than unity and rises slowly for both cases. The ratio for $Ri=0.01$ is slightly smaller than that of $Ri=0.005$, which indicates that the effects of the weakened streamwise flow is slightly more influencing for $Ri=0.01$.

Comparing the results between the right wall and left wall, the enhancement of heat transfer is more intensive on the right wall which is thought to be the results of increased streamwise

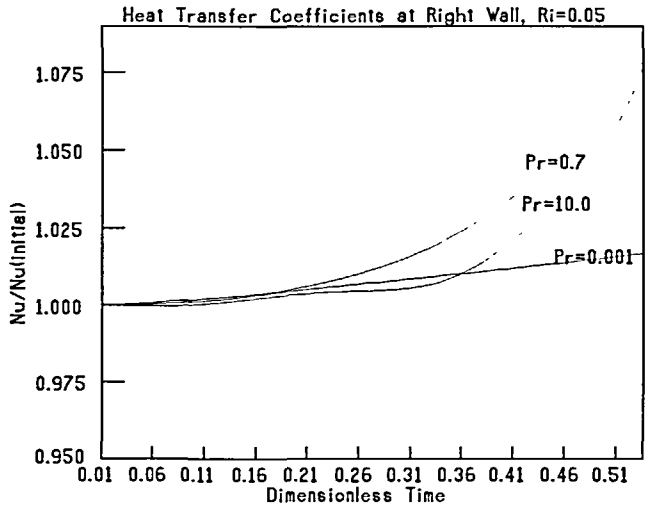

Figure 22 Nusselt Number ratio as a function of time at the right wall for $Ri=0.05$

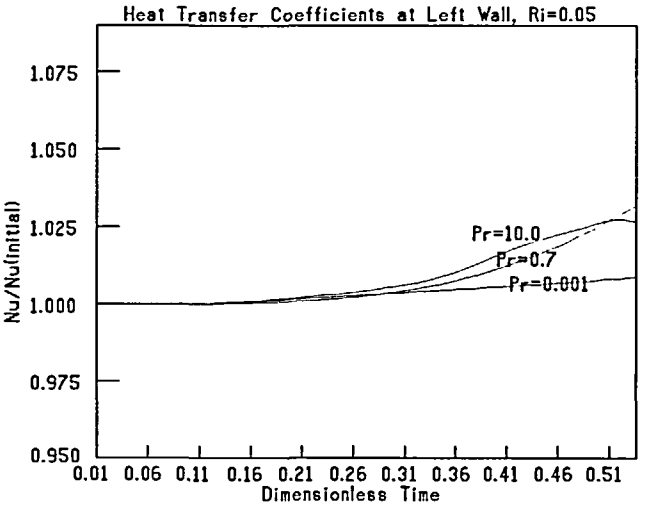

Figure 23 Nusselt Number ratio as a function of time at the left wall for $Ri=0.05$

flow induced by the buoyancy force. Again we need to investigate the effects of the Pr number on the Nu number ratio for both walls. Following the same trend, the order of magnitude of enhancement is definitely higher for the right wall. For both walls, the enhancement is the lowest for the liquid metals ($Pr=0.001$). This is believed to be caused by the extremely high thermal conductivity of the liquid metal which tends to minimize the convection mechanisms due to transition and buoyancy forces. Heat conduction also tends to stabilize the instability in the system. For the right wall, it is shown in *Figure 22* that the gaseous fluids ($Pr=0.7$) benefit the most in a transition flow. This is probably due to relatively higher viscosity of the liquids ($Pr=10$). It is well known that viscosity tends to stabilize the flow and therefore the transition process in

the liquids ($Pr=10$) is slower and less intense than the gaseous fluids ($Pr=0.7$). This explains that the Nu number ratio is the highest for the gaseous fluids ($Pr=0.7$) in *Figures 22* and *23*.

CONCLUSION

The transition phenomena in a mixed-convection flow can be significantly different from those in the isothermal flow. An initial K-type disturbances may not produce the K-type transition as in an isothermal flow. Instead the 2-D TS waves grow continuously and trigger the lower mode waves to grow. There exist thresholds in the lower-mode growing process. The 2-D TS wave ($k_x=1,k_z=0$) extracts energy from the mean flow and triggers the lower-mode disturbances once itself gains enough energy. It is found that all disturbances waves grow in a very short time. This implies that a fully-developed mixed-convection flow may not exist between two vertical plates. Those energetic disturbances keep taking energy from the mean flow and a fully-developed flow can hardly exist.

The streamwise vortex pattern is different from that in an isothermal flow. The streamwise vortices are concentrated near the left of the centerline between the walls. The vortex system is distorted and sometimes lifted up as the Ri number is increased. As the Ri number approaches 0.05, a hairpin vortex pattern is most likely to form. Visualization of the flow by particles indicates that the λ vortices are formed. Their pattern is a staggered one and no well-aligned isothermal K-type breakdown pattern was observed. Large-scale periodic motions are found in the streamwise direction.

In general, the calculated Nu number is greater than that of the initial laminar flow. The ratio of the former to the latter increases with time and the rate of increase is proportional to the Ri number, which is a result of the competition between the nonlinear transition mechanism and the buoyancy induced streamwise motion of relaminarization. The enhancement of heat transfer is more intense at the right wall boundary were the buoyancy induced flow is in the streamwise direction. Near the left wall, the buoyancy tends to weaken the forced flow or even induce a reverse flow, which reduces the Nu number. For various Pr numbers which represent three fluid groups, the gaseous fluids ($Pr=0.7$) seem to possess the highest heat transfer enhancement in the transitional mixed-convection flow. The liquid metals have the lowest heat transfer increase which is mainly due to the stabilizing effect of the high thermal conductivity value. The liquids ($Pr=10$) fall below the gases because the higher viscosity of the liquid tends to stabilize the flow.

Transition can be delayed due to the favourable pressure gradient induced by the buoyancy force. Transition can also be promoted if buoyancy induces an adverse pressure gradient. It is also found that the buoyancy can control the transition even at the nonlinear stage. The effectiveness of transition control by buoyancy, relies on the existence of a mixed-convection flow. The option of using buoyancy to control the transition will not be applicable in a forced-convection flow.

ACKNOWLEDGEMENT

The authors like to thank Dr R. D. Moser and Dr S. P. Spalart of the NASA Ames Research Center for useful information and discussions. The supercomputing environment at the NCSA Facility provided the indispensable tool for this study.

BIBLIOGRAPHY

1 Schubauer, G. B. and Skramstad, H. K. Laminar boundary-layer oscillations and transition on a flat plate, *J. Res. Natl Bur. Stand.*, **38** no. 2, 251–292 (1947)

2 Strazisar, A. J., Reshotko, E. and Prahl, J. M. Experimental study of the stability of the heated laminar boundary layers in water, *J. Fluid. Mech.*, **83**, 225–247 (1977)

3 Krist, S. E. and Zang, T. A. Numerical simulation of Channel Flow transition, *NASA Technical Paper 2667*, (1987)
4 Klebanoff, P. S., Tidstrom, K. D. and Sargent, L. M. The three-dimensional natural of boundary-layer instability, *J. Fluid Mech.*, **12**, 1 (1962)
5 Craik, A. D. D. Non-linear resonant instability in boundary layers, *J. Fluid Mech.*, **50**, 393 (1971)
6 Herbert, T. Secondary instability of plane channel flow to subharmonic three-dimensional disturbances, *Phys. Fluids*, **26**, 871 (1981)
7 Spalart, R. P. Numerical simulation of boundary layers transition, *9th Int. Conf. Num. Meth. in Fluid Dyn.*, Paris (1984)
8 Spalart, R. P. and Yang, K. S. Numerical study of Ribbon-induced transition in Blasius flow, *J. Fluid Mech.*, **178**, 345–365 (1987)
9 Mucoglu, A. and Chen, T. S. Wave instability of mixed convection flow along a vertical flat plate, *Numer. Heat Transfer*, **1**, 267 (1978)
10 Chen, T. S. and Mucoglu, A. Wave instability of mixed convection flow over a horizontal flat plate, *Int. J. Heat Mass Transfer*, **22**, 185 (1979)
11 Gebhart, B., Jaluria, Y., Mahajan, R. and Sammakia, B. *Buoyancy-induced flows and transport*, Hemisphere Book Publishing Co., New York (1988)
12 Zang, T. A. and Hussaini, M. Y. Numerical experiments on the stability of controlled boundary layers, *NASA Contractor Report 181649, ICASE Report No. 88-20* (1988)
13 Orszag, S. A. and Kells, L. C. Transition to turbulence in plane Poiseuille and plane Couette flow, *J. Fluid Mech.*, **96**, 159 (1980)
14 Ghaddar, N. K., Magen, M., Mikic, B. B. an Patera, A. T. Numerical investigation of incompressible flow in grooved channels. Part 2 Resonance and oscillatory heat-transfer enhancement, *J. Fluid Mech.*, **168**, 541 (1986)
15 Lee, L. H. and Reynold, W. C. On the approximate and numerical solution of Orr-Sommerfeld problems, *Quart. J. Mech. Appl. Math.*, **20**, 1 (1967)
16 Leonard, A. Divergence-free vector expansions for 3-D flow simulations, *Bull. Amer. Phys. Soc. 26*, 1247 (1981)
17 Moser, R. D., Moin, P. and Leonard, A. A spectral numerical method for the Navier-Stokes equations with applications to Taylor-Couette flow, *J. Comp. Phys.*, **52**, 524–544 (1983)
18 Hao, C. C. Numerical investigation of 3-D transitional channel flows with heat transfer, PhD dissertation, Washington State University (1990)
19 Hao, C. C. and Chung, J. N. Flow structures and heat transfer during transition in perturbed mixed-convection channel flows, submitted to *Numerical Heat Transfer A* (1993)
20 Yao, L. S. Is a fully-developed and non-isothermal flow possible in a vertical pipe? *Int. J. Heat and Mass Transfer*, **30**, 707–716 (1987)
21 Paterson, G. S. and Orszag, S. A. Spectral calculations of isotropic turbulence: efficient removal of aliasing interactions, *Phys. Fluids*, **14**, 2538 (1971)
22 Spalart, R. P. Numerical study of waves in nonparallel flows. *Bulletin of The American Physical Society*, **34**, 2335 (1989)